Asociación Argentina
de Mecánica Computacional

Mecánica Computacional Vol XXIX, págs. 2819-2837 (artículo completo)
Eduardo Dvorkin, Marcela Goldschmit, Mario Storti (Eds.)
Buenos Aires, Argentina, 15-18 Noviembre 2010

NUMERICAL TESTS FOR SHEAR MECHANISMS BASED ON TWO DIFFERENT CALIBRATION POINTS

Lucival Malcher[a,b], Fábio J. P. Reis[a], Francisco M. Andrade Pires[a], J. M. A. César de Sá[a] and Filipe X. C. Andrade[a]

[a]*IDMEC – Institute of Mechanical Engineering, Faculty of Engineering, University of Porto, Rua Dr. Roberto Frias, Porto 4200-465, Portugal*

[b]*lucival.malcher@fe.up.pt*

Keywords: void growth mechanism, shear mechanism, ductile fracture, crack formation, calibration point, low stress triaxiality.

Abstract. In this paper, a numerical comparative study for shear mechanisms is performed, based on two different calibration points. The assessment is motivated due to the fact that the accuracy of the results obtained by coupled damage models is strongly dependent on the calibration point. Hence, the numerical results obtained by these models are more realistic and in agreement with experimental evidence when the external loading conditions are close to the calibration point. By the way, shear mechanisms proposed by Xue and Nahshon & Hutchison were selected and added into damage variable of Gurson-Tvergaard-Needleman model (GTN), in order to give ability to predict crack formation when shear loading condition is presented. In the first part of this paper, both mechanisms are presented as well as the GTN model. Besides that, the numerical strategy is introduced, based on an implicit integration algorithm. In the following section, a point in high and other in low stress triaxialities are taken as calibration points and by an inverse method, the material parameters are obtained. In order to analyze the dependence of the results in relation to the calibration point, numerical tests are carried out for pure shear and combined shear/tensile loading conditions using first, the material parameters obtained by the first calibration point and then, using the properties which resulted by the second calibration point. Both numerical results are compared with experimental data and the ability to predict the correct fracture location. At the end, the equivalent plastic strain and displacement at fracture are analyzed for each calibration condition. The numerical tests have shown that for the loading conditions applied, the material properties obtained by the shear calibration point was more appropriate than the material properties taken for high stress triaxiality calibration point.

1 INTRODUCTION

The fracture in metals is an important subject to be improved, regarding the ability to predict the correct location of crack initiation in machine components and rupture in general structures. This phenomenon can be studied by its separated evolution contribution as the initiation and growth of general micro defects which is induced by large deformations. Some researchers like McClintock (1968) and Rice & Tracey (1969) developed pioneering work undertaken on the subject, where the nature of defect was taken into account the study of ductile damage by analyzing its geometry in a continuous matrix.

The degradation of material properties is an irreversible process and starts from the formation of micro defects which can be voids, cracks and others, that already exist or that will be formed in the material matrix. However, the evolution of material degradation is dependent on macroscopic loading conditions which can cause a volumetric void growth such as in tensile loading condition or a preferential elongation of micro defects which can be observed in pure shear loading conditions. The ductile fracture phenomenon can be described, based on a micromechanical analysis of micro cavity growth, especially for the fracture computation within local approaches of fracture, (see Pineau, 1981; Rousselier, 1987; Besson et al., 2001) or based on the Continuum Damage Mechanics theory and a thermodynamic framework, either phenomenological or micromechanically based, as Lemaitre (1985) for damage caused by plastic flow, Chaboche (1984) and Murakami & Ohno (1981) for creep damage, Krajčinović & Fonseka (1981) on micromechanical grounds.

The formulations proposed by Lemaitre and Gurson are the most important coupled damage ductile models to describe the above two methodologies (see Chaboche et al., 2006). Since then, motivated by the limitations of these classical models, such as in prediction of the correct fracture location or in determination of the correct values of the internal variables at fracture, many researchers have proposed improvements in both methodologies, by introducing more effects in the constitutive formulation or in the damage evolution law like the pressure effect, temperature, Lode angle dependence, viscoplastic effects, crack closure effect, shear mechanisms, among others (Tvergaard & Needleman, 1984; Rousselier, 1980 and 2001; Xue, 2007; Nahshon & Hutchinson, 2008; Lemaitre & Chaboche, 1990; Chaboche, 2003; Andrade Pires et al., 2004; Chaboche et al., 2006 ; Besson, 2010).

These classical coupled damage models have the ability to predict the correct fracture location under a specific range of stress triaxialities (see Xue, 2007; Nahshon et al.; 2008; Teng, 2008) and are extremely accurate for loading conditions close to the calibration point (see Malcher, 2010). For example, within range of high levels of stress triaxialities, where the spherical void growth is the predominant mechanism, the models based on Gurson theory, like the Gurson-Tvergaard-Needleman model (GTN), have good performance in prediction of fracture location and parameters in fracture as equivalent plastic strain and displacement. However, under shear

dominated loads, where failure is mainly driven by the shear localization of plastic strain of the inter-voids ligaments due to void rotation and distortion, the model does not perform well, (see Engelen, 2005; Chaboche, 2006). Figure 1 illustrates the ductile failure mechanism, which can occur by internal necking (Figure 1a), where the large primary voids are formed due to high stress triaxiliaty and the inter ligaments are done mainly by a sharp volumetric or by void sheeting (Figure 1b), where primary voids remain small due to low stress triaxiality and the inter ligament occurs by mainly elongation of voids and formation of secondary voids in strain localization bands.

Due to these two types of ductile failure mechanisms, it is expected that the population of micro defects, that can be nucleated, would be higher in void sheeting than in internal necking.

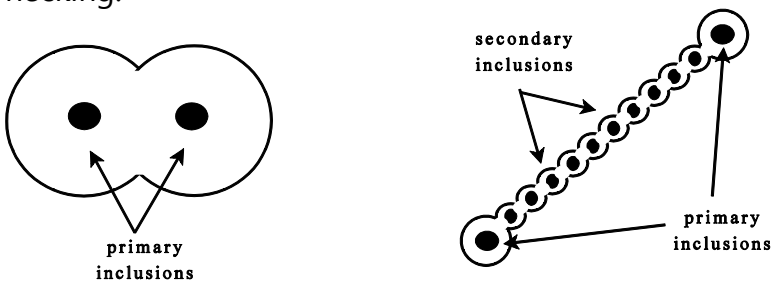

Figure 1. Schematic representation of ductile failure mechanism (a) internal necking and (b) void sheeting. Adapted from Besson, (2010).

2 CONSTITUTIVE MODEL

Regarding the work initially developed by Rice and Trace (1969) in order to analysis the behaviour of an isolated void, Gurson (1977) proposed a theory to describe an internal degradation of material in presence of the finite strain which is the first micromechanical based model for ductile damage and fracture. Gurson assumes as internal degradation mechanism the appearance of micro voids associated with a large plastic deformation, which leads a yield surface that depends on the hydrostatic pressure and porosity. The evolution of the damage parameters by Gurson is established by assuming a spherical cavity imbibed into a cubic rigid-plastic matrix without hardening and the volume void fraction, which plays the damage role parameters is defined as a ratio between the volume of voids and the volume of the representative volume element.

$$f = \frac{V_{void}}{V_{RVE}} \tag{1}$$

where f represents the void volume fraction, V_{void} is the volume of the void and V_{RVE} denotes the representative volume element.

The Tvergaard–Needleman proposition (GTN) (see Tvergaard and Needleman, 1984) is one of the most famous versions of the Gurson model. The GTN's model

assumes isotropic hardening and isotropic damage, which is represented by the effective porosity, f^*. The constitutive formulation for GTN's model can be better expressed as:

$$\Phi(\boldsymbol{\sigma}, k, f) = J_2(\boldsymbol{S}) - \frac{1}{3}\left\{1 + q_3.f^{*2} - 2.q_1.f^*.\cosh\left(\frac{q_2.3.p}{2.\sigma_y}\right)\right\}.{\sigma_y}^2 \tag{2}$$

where, J_2 represents the second invariant of the deviatoric stress tensor, p is the hydrostatic pressure, σ_y represents the yield stress and the parameters q_1, q_2 and q_3 are introduced to bring the model predictions into closer agreement with full numerical analyses of a periodic array of voids.

The damage evolution, in this formulation, is reproduced by three simultaneous or successive mechanisms that can be described as the nucleation, growth and coalescence of voids as:

$$f^* = \begin{cases} f, & f < f_c \\ f_c + \left(\frac{1}{q_1} - f_c\right)\frac{(f - f_c)}{(f_f - f_c)}, & f \geq f_c \end{cases} \tag{3}$$

where, f^* represents the effective damage, f_c denotes the critical volume void fraction and f_f is the volume void fraction at fracture. The effective damage is determined based on both nucleation and growth mechanisms if the volume void fraction is less than critical value. The coalescence is active only if the volume void fraction is higher than the critical value. The volume void fraction rate, $\dot{f}$, is a sum of the nucleation and growth mechanism as.

$$\dot{f} = \dot{f}^n + \dot{f}^g \tag{4}$$

The nucleation mechanism can be driven by either the plastic strain or the hydrostatic pressure. Equation 5 represents the nucleation mechanism based on the equivalent plastic strain:

$$\dot{f}^n = \frac{f_{\mathrm{N}}}{s_{\mathrm{N}}.\sqrt{2\pi}}.\exp\left[-\frac{1}{2}\left(\frac{\overline{\varepsilon}^p - \varepsilon_{\mathrm{N}}}{s_{\mathrm{N}}}\right)^2\right]\dot{\overline{\varepsilon}}^p \tag{5}$$

where, f_{N} represents the volume fraction of all second-phase particles with potential for microvoid nucleation, ε_{N} and s_{N} are the mean strain/pressure for void nucleation and its standard deviation. The variable $\overline{\varepsilon}^p$ represents the equivalent plastic strain and $\dot{\overline{\varepsilon}}^p$ is the rate of the accumulated plastic strain. The nucleation mechanism is valid only if the hydrostatic pressure is great to zero, $p > 0$. If $p \leq 0$, the nucleation mechanism rate is equal to zero. The evolution of the volume void fraction by Gurson is assumed based on mass conservation law, a rigid plastic material and the plastic incompressibility and is defined as:

$$\dot{f}^g = \dot{\varepsilon}_v^p.(1 - f) \tag{6}$$

where, the plastic strain rate contributions is represented by $\dot{\varepsilon}_v^p$.

2.1 Shear mechanism

Regarding the limitation of the Gurson original model in prediction failure when void sheeting mechanism plays the main role, researchers as Xue (2007), Nahshon & Hutchinson (2008), Butcher et al. (2009) have suggested the introduction of another mechanism as shear, in the evolution law of the Gurson's damage parameter. Both researchers have initially formulated shear mechanisms based on phenomenological and geometrical aspects resulting in expression dependent on the equivalent strain and its rate and a Lode angle function. Xue (2008), based on the volume conservation of a cubic cell, has proposed that the rate of the shear damage can be written by:

$$\dot{D}_{shear} = q_4 . g_0 . f^{q_5} . \varepsilon_{eq} . \dot{\varepsilon}_{eq} \tag{7}$$

where, q_4 and q_5 are geometrical parameters and can be defined according to two or three dimensional problem. For two dimensional problem, $q_4 = \frac{3}{\sqrt{\pi}}$ and $q_5 = (1/2)$ and for three dimensional problem, $q_4 = \frac{3}{2}\left(\frac{6}{\pi}\right)^{(1/3)}$ and $q_5 = (1/3)$. ε_{eq} and $\dot{\varepsilon}_{eq}$ represent the equivalent strain and its rate, respectively. g_0 denotes the Lode angle function that by Xue is defined as

$$g_0 = \left(1 - \left|\bar{\theta}\right|\right) \tag{8}$$

where, $\bar{\theta}$ is the normalized Lode angle, which can be expressed as $\bar{\theta} = 1 - \frac{2}{\pi}\text{acos}(\xi)$ and ξ is the normalized third invariant, which is a ratio between the third invariant of the deviatoric stress tensor, $r = [(27/2).\det \boldsymbol{S}]^{1/3}$, and the von Mises equivalent stress, $q = \sqrt{(3/2)\boldsymbol{S}:\boldsymbol{S}}$.

Nahshon & Hutchinson (N&H) have suggested a shear mechanism based on phenomenological aspects that can be written as (see Nahshon et al, 2008):

$$\dot{D}_{shear} = k . f . g_0 . \frac{\boldsymbol{S}:\boldsymbol{\varepsilon^p}}{q} \tag{9}$$

where, k is a material parameter and needs to be calibrated. $\boldsymbol{\varepsilon^p}$ denotes the plastic strain tensor. The Lode angle function by Nahshon et al. (2008) is defined as:

$$g_0 = (1 - \xi^2) \tag{10}$$

Thus, the damage internal variable rate (Equation 4) can be re-written according to Equation 11.

$$\dot{f} = \dot{f}^n + \dot{f}^g + \dot{D}_{shear} \tag{11}$$

3 NUMERICAL INTEGRATION ALGORITHM

Regarding an implicit solution, algorithms based on operator split methodology are especially suitable for the numerical integration of the evolution problem and

have been widely used in computational plasticity (see Simo & Hughes, 1998; De Souza Neto et al., 2008). This method, which is used here, consists of splitting the problem in two parts: an elastic predictor, where the problem is assumed to be elastic and, a plastic corrector, in which the system of residual equations comprising the elasticity law, plastic consistency and the rate equations is solved, taking the results of the elastic predictor stage as initial conditions. In the case of the yield condition has been violated, the plastic corrector stage is initiated and the Newton- Raphson procedure is used to solve the discretised equations. The Newton-Raphson procedure was chosen motivated by the quadratic rates of convergence achieved which results in return mapping procedures computationally efficient (see Simo & Hughes, 1998; De Souza Neto et al., 2008). The overall algorithm for numerical integration is summarized in Box 1.

Box 1. Fully implicit Elastic predictor/Return mapping algorithm

(i) Evaluate the elastic trial state: Given the incremental strain $\Delta\varepsilon$ and the state variables at t_n:

$$\boldsymbol{\varepsilon}_{n+1}^{e\,trial} = \boldsymbol{\varepsilon}_n^e + \Delta\boldsymbol{\varepsilon} \quad ; \quad \bar{\varepsilon}_{n+1}^{p\,trial} = \bar{\varepsilon}_n^p \quad ; \quad R_{n+1}^{trial} = R_n$$

$$f_{n+1}^{trial} = f_n \quad ; \quad \boldsymbol{S}_{n+1}^{trial} = 2G\boldsymbol{\varepsilon}_{n+1}^{e\,trial} \quad ; \quad p_{n+1}^{trial} = K\varepsilon_{v\,n+1}^{e\,trial}$$

$$\sigma_y^{trial} = \sigma_y\left(R_{n+1}^{trial}\right)$$

(ii) Check plastic admissibility:

IF $\Phi^{trial} = J_2^{trial} - \frac{1}{3}.\left[1 + q_3.{f_{n+1}^{trial}}^2 - 2.q_1.f_{n+1}^{trial}.\cosh\left(\frac{3.q_2.p_{n+1}^{trial}}{2.\sigma_y^{trial}}\right)\right].\left(\sigma_y^{trial}\right)^2 \leq 0$ THEN

set $(\cdot)_{n+1} = (\cdot)_{n+1}^{trial}$ ***(elastic step)*** and go to *(v)*

ELSE go to (iii)

Continue Box 1.

(iii) Return mapping ***(plastic step)***: *Solve the system of equations below for* $\Delta\gamma, p_{n+1}, f_{n+1}$ and R_{n+1}, *using Newton-Raphson method:*

$$\begin{Bmatrix} \dfrac{J_{2_{n+1}}^{trial}}{(1+2G.\Delta\gamma)^2} - \dfrac{1}{3}.\left[1 + q_3.{f_{n+1}}^2 - 2.q_1.f_{n+1}.\cosh\left(\dfrac{3.q_2.p_{n+1}}{2.\sigma_y}\right)\right].\sigma_y^2 \\ p_{n+1} - p_{n+1}^{trial} + \Delta\gamma.K.\sigma_y.q_1.q_2.f_{n+1}.\sinh\left(\dfrac{3.q_2.p_{n+1}}{2.\sigma_y}\right) \\ f_{n+1} - f_{n+1}^{trial} - \Delta f^n - \Delta f^g - \Delta D_{shear} \\ R_{n+1} - R_{n+1}^{trial} - \Delta R \end{Bmatrix} = \begin{Bmatrix} 0 \\ 0 \\ 0 \\ 0 \end{Bmatrix}$$

where,

$$\Delta f^n = \frac{f_N}{S_N\sqrt{2.\pi}}.\exp\left[-\frac{1}{2}\left(\frac{\bar{\varepsilon}_{n+1}^p - \varepsilon_N}{S_N}\right)^2\right].\Delta\bar{\varepsilon}^p$$

$$\Delta f^g = (1-f_{n+1}).\Delta\gamma.\sigma_y.q_1.q_2.f_{n+1}.\sinh\left(\frac{3.q_2.p_{n+1}}{2.\sigma_y}\right)$$

$$\Delta D_{shear} = \begin{cases} q_4.\left(1-\left|\bar{\theta}_{n+1}^{trial}\right|\right).f_{n+1}^{q_5}.\bar{\varepsilon}_{n+1}^p.\Delta\bar{\varepsilon}^p, & if\ Xue's\ mechanism \\ k.f_{n+1}.\left(1-{\xi_{n+1}^{trial}}^2\right).\Delta\bar{\varepsilon}^p, & if\ Nahshon's\ mechanism \end{cases}$$

$$\Delta R = \frac{\Delta\gamma}{(1-f_{n+1})}.\left\{q_1.q_2.f_{n+1}.p_{n+1}.\sinh\left(\frac{3.q_2.p_{n+1}}{2.\sigma_y}\right) + \frac{2}{3}.\sigma_y.\left[1+q_3.{f_{n+1}}^2 - 2.q_1.f_{n+1}.\cosh\left(\frac{3.q_2.p_{n+1}}{2.\sigma_y}\right)\right]\right\}$$

(iv) Update the others state variables:

$$\boldsymbol{\varepsilon}_{n+1}^e = \boldsymbol{\varepsilon}_{n+1}^{e\ trial} - \Delta\gamma.\left[\frac{\boldsymbol{S}_{n+1}^{trial}}{(1+2G.\Delta\gamma)} + \frac{1}{3}.\sigma_y.q_1.q_2.f_{n+1}.\sinh\left(\frac{3.q_2.p_{n+1}}{2.\sigma_y}\right).\boldsymbol{I}\right]$$

$$\boldsymbol{S}_{n+1} = \frac{\boldsymbol{S}_{n+1}^{trial}}{(1+2G.\Delta\gamma)}$$

$$\boldsymbol{\sigma}_{n+1} = \boldsymbol{S}_{n+1} + p_{n+1}.\boldsymbol{I}$$

$$\Delta\bar{\varepsilon}^p = \Delta\gamma.\sqrt{\frac{2}{3}\left\{\frac{\boldsymbol{S}_{n+1}^{trial}:\boldsymbol{S}_{n+1}^{trial}}{(1+2G.\Delta\gamma)^2} + \frac{1}{3}\left[\sigma_y.q_1.q_2.f_{n+1}.\sinh\left(\frac{3.q_2.p_{n+1}}{2.\sigma_y}\right)\right]^2\right\}}$$

$$\bar{\varepsilon}_{n+1}^p = \bar{\varepsilon}_{n+1}^{p\ trial} + \Delta\bar{\varepsilon}^p$$

(v) Exit

3.1 The consistent tangent operator

Under elastic loading condition, the tangent operator for this constitutive formulation is the standard linear elasticity tensor. Nevertheless, for the plastic step, the elasto-plastic tangent operator is obtained by the linearization procedure of the above system of residual equations. Hence, the first step for determining the operator is to differentiate the stress tensor update expression:

$$\boldsymbol{\sigma}_{n+1} = \frac{\boldsymbol{S}_{n+1}^{trial}}{[1 + 2G.\Delta\gamma]} + p_{n+1}.\boldsymbol{I} \tag{12}$$

After some algebraic manipulation, the above equation can be re-written by differentiate form as:

$$\mathrm{d}\boldsymbol{\sigma}_{n+1} = \frac{2G}{[1 + 2G.\Delta\gamma]}.\mathrm{d}\boldsymbol{\varepsilon}_{d\ n+1}^{e\ trial} - \left\{\frac{2G}{[1 + 2G.\Delta\gamma]}\right\}^2.\boldsymbol{\varepsilon}_{d\ n+1}^{e\ trial}.\mathrm{d}\Delta\gamma + \mathrm{d}p_{n+1}.\boldsymbol{I} \tag{13}$$

The terms $\mathrm{d}\Delta\gamma$ and $\mathrm{d}p_{n+1}$ can be obtained by the linearization procedure of the residual system of equations. After some algebraic manipulation, the term $\mathrm{d}\Delta\gamma$ and $\mathrm{d}p_{n+1}$ can be written as:

$$\begin{aligned}
\mathrm{d}\Delta\gamma &= -C_{1,1}.\frac{\partial r_{\Delta\gamma}}{\partial \boldsymbol{\varepsilon}_{d\ n+1}^{e\ trial}} - C_{1,2}.\frac{\partial r_p}{\partial \boldsymbol{\varepsilon}_{v\ n+1}^{e\ trial}} - C_{1,3}.\frac{\partial r_f}{\partial \boldsymbol{\varepsilon}_{d\ n+1}^{e\ trial}} \\
\mathrm{d}p_{n+1} &= -C_{2,1}.\frac{\partial r_{\Delta\gamma}}{\partial \boldsymbol{\varepsilon}_{d\ n+1}^{e\ trial}} - C_{2,2}.\frac{\partial r_p}{\partial \boldsymbol{\varepsilon}_{v\ n+1}^{e\ trial}} - C_{2,3}.\frac{\partial r_f}{\partial \boldsymbol{\varepsilon}_{d\ n+1}^{e\ trial}}
\end{aligned} \tag{14}$$

where, the matrix **C** is the inversion matrix of the differentiation residual equations in order to each variable of the problem. Furthermore, the elasto-plastic operator can be determined as:

$$\mathbb{D}^{ep} = \frac{\mathrm{d}\boldsymbol{\sigma}_{n+1}}{\mathrm{d}\boldsymbol{\varepsilon}_{n+1}^{e\ trial}} \tag{15}$$

4 CALIBRATION PROCEDURE

In order to determine the materials parameters for GTN model and GTN model with shear mechanism coupled, two different calibration points are suggested, regarding the accuracy of the numerical results. First one, the material parameters will be determined based on a usual calibration point, which the *smooth cylindrical bar* is taken. After that, a second point is suggested to be used as calibration point and again, all material parameters are calibrated based on a so called "*butterfly specimen*" under pure shear loading condition. In both cases, the hardening law, $\sigma_y(R)$, for the undamaged model is determined as well as the set of parameters for nucleation of micro void mechanism $[f_N, S_N, \varepsilon_N]$ and the critical value for the damage variable, f_c. The accuracy of both shear mechanisms will be assessed taken hand a material weakly dependent on the Lode angle, as a steel 1045. Furthermore, in both cases, the

numerical tests are conducted for two different loading conditions: pure shear and shear/tensile loading conditions.

4.1 Geometry and mesh definition

Regarding the material properties for the first calibration point, a *classical smooth bar specimen* is used and Figure 2a presents the dimensions employed. In order to trigger necking, a dimensional reduction of 5% in the central diameter of the specimen is used. Besides that, based on the experimental data, a gauge section of 20.6 mm is also used. The standard eight-nodded axsymmetric quadrilateral element, with four Gauss integration points, is adopted. The initial mesh discretisation is illustrated in Figure 2b, where only one symmetric quarter of the problem, with the appropriate symmetric boundary conditions imposed to the relevant edges, is modelled. A total number of 1800 elements have been used in the discretisation of the smooth specimen, amounting to a total of 5581 nodes.

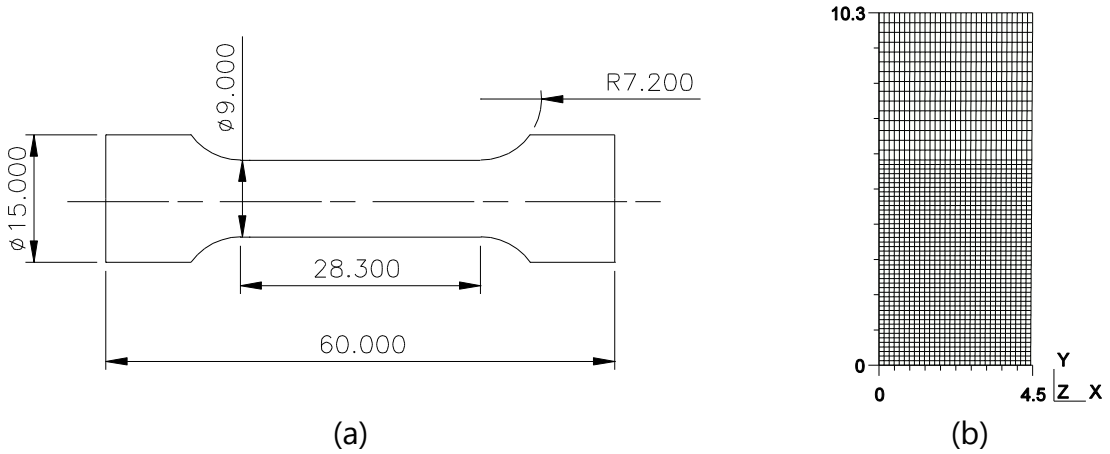

Figure 2. (a) The geometry for the smooth bar specimen. Dimension in (mm). Taken from Teng (2008). (b) Finite element mesh, regarding the gauge section.

For the second calibration point and all numerical tests that will be presented, a *butterfly specimen* is used. The specimen was initially designed by Bai (2008) and the geometry and general dimensions can be verified by Figure 3. In this case, a three dimensional finite element mesh of 3392 twenty nodded elements, with nine Gauss integration points, is used amounting to 17465 nodes.

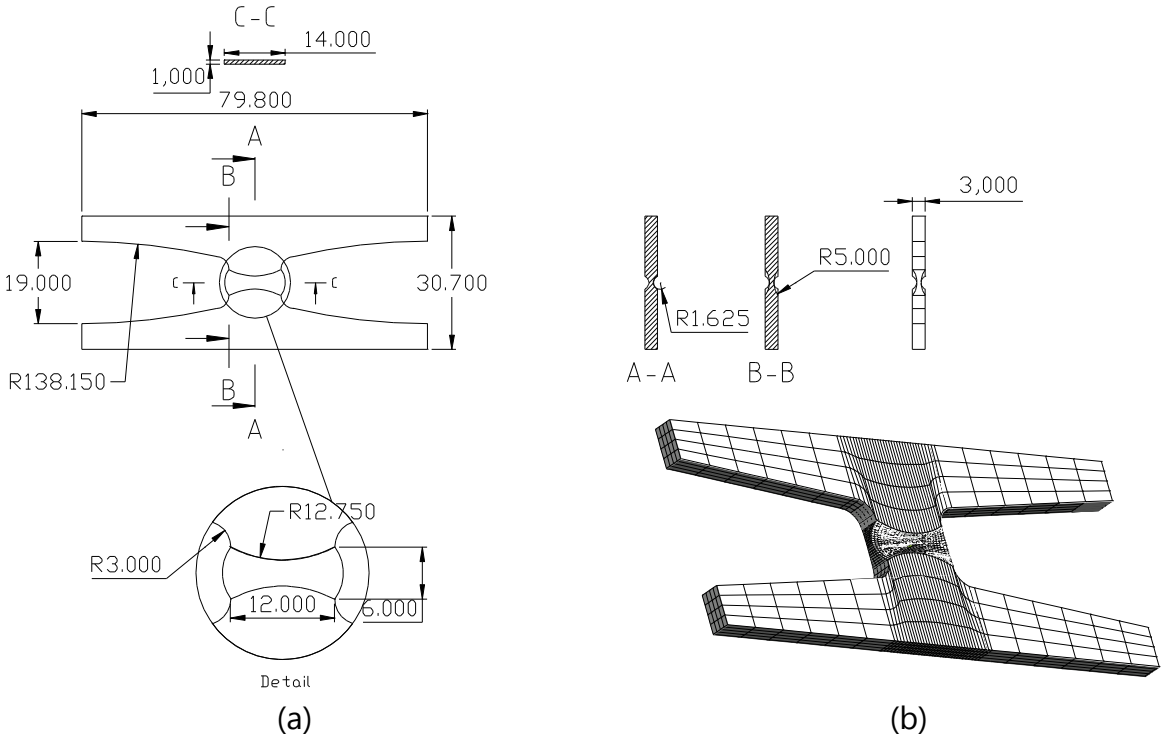

(a) (b)

Figure 3. (a) The geometry for butterfly specimen. Dimension in (mm). Taken from Bai (2008). (b) Finite elements mesh for butterfly specimen.

4.2 First Calibration Point: smooth bar specimen (tensile loading condition)

In the present section the hardening law, $\sigma_y(R)$, for the undamaged model is determined as well as the set of parameters for nucleation of micro void mechanism $[f_N, S_N, \varepsilon_N]$ and the critical value for the damage variable, f_c. Through experimental tests conducted by Bai 2008, the reaction versus displacement curve is determined as well as the stress-strain curve for an elasto-plastic model of von Mises type. The inverse method is adopted in order to calibrate the material parameters for coupled damage model by forcing the numerical solution to be, as close as possible to the experimental results. Figure 4a shows the reaction curve for the model determined after the application of inverse method. A good agreement between the experimental and numerical results can be observed. Furthermore, the critical volume void fraction is also determined in the point where the model attains the displacement to fracture, experimentally observed (see Figure 4b). The critical value obtained is $f_c = 0.076$.

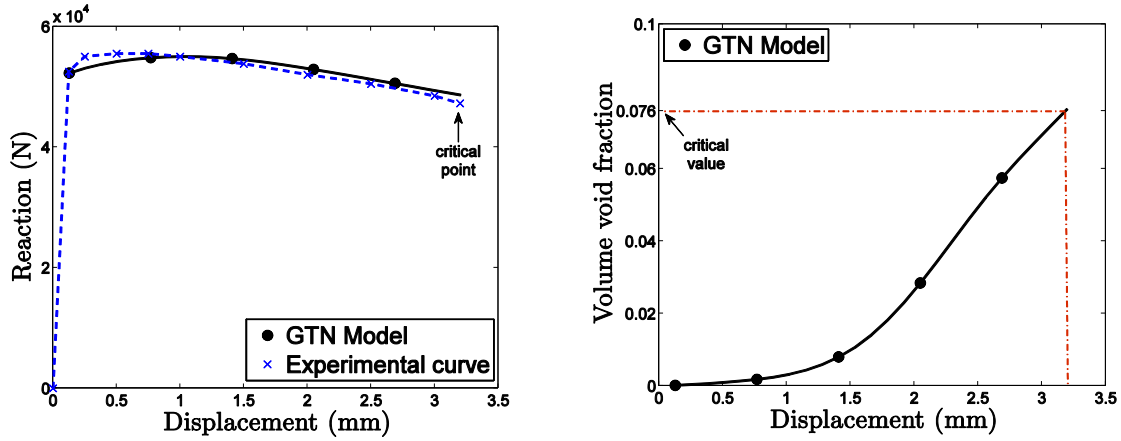

Figure 4. (a) Reaction versus displacement curve. (b) Critical volume voids fraction parameter

The results of the calibration procedure, in terms of stress-strain curve, can also be observed in Figure 5, where the curves, for uncoupled and coupled damage models, were determined.

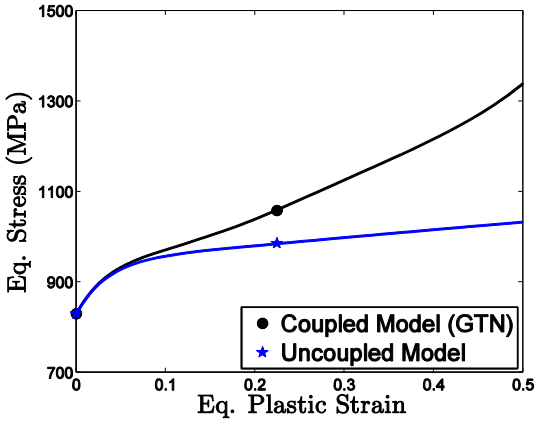

Figure 5. Stress-strain curves determined for an uncoupled and coupled models.

The material properties and others parameters related to the micro void nucleation mechanism obtained by employing an inverse method are listed in Table 1:

Material	f_N	S_N	ε_N	q_1	q_2	q_3	f_c	E (MPa)	υ
GTN	0.05	0.2	0.1	1.5	1.0	2.25	0.076	220.000	0.33

Table 1: Materials properties and parameters related to nucleation of micro-void mechanism for steel 1045. Based on the first calibration point.

4.3 Second Calibration Point: butterfly specimen (pure shear loading condition)

In this calibration point, also the hardening law, $\sigma_y(R)$, for the undamaged model is determined as well as the set of parameters for nucleation of micro void mechanism $[f_N, S_N, \varepsilon_N]$ and the critical value for the damage variable, f_c. The butterfly

specimen is here used under pure shear loading condition and the displacement to fracture, experimental determined, was suggested by Bai (2008). An inverse method is also adopted, regarding the calibration of the parameters by forcing the numerical results to be as close as possible to the experimental data. A critical damage value is suggested by each shear mechanism and the result of the second calibration can be observed by Figure 6.

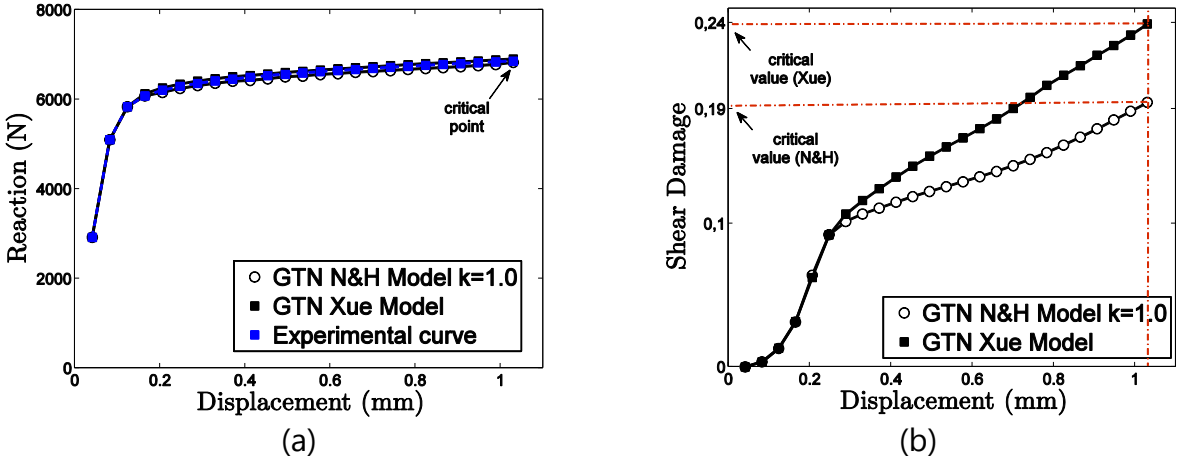

(a) (b)

Figure 6. (a) Reaction versus displacement curve. (b) Shear damage parameter.

In terms of stress-strain curve, it can also be observed in Figure 7, where the curves, for uncoupled and coupled damage models, were determined.

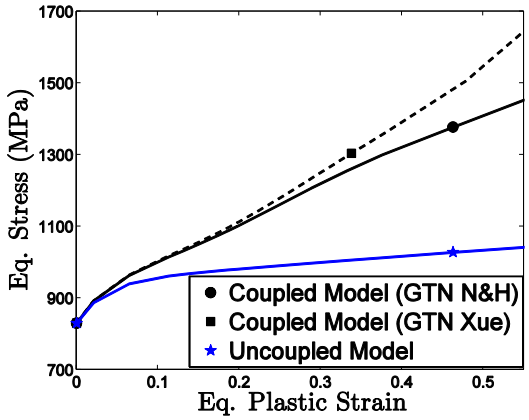

Figure 7. Stress-strain curves determined for an uncoupled and coupled models.

The material properties and others parameters related to the micro void nucleation mechanism obtained by employing an inverse method are also listed in Table 2:

Material	f_N	S_N	ε_N	q_1	q_2	q_3	f_c	E (MPa)	υ
N&H	0.10	0.15	0.1	1.5	1.0	2.25	0.19	220.000	0.33
Xue	0.10	0.15	0.1	1.5	1.0	2.25	0.24	220.000	0.33

Table 2: Materials properties and parameters related to nucleation of micro-void mechanism for steel 1045. Based on the second calibration point.

5 NUMERICAL RESULTS

Regarding a consistent analysis for the accuracy of both shear mechanisms, some numerical tests are performed using the *butterfly specimen* taken hand the material parameters determined based on the first calibration point and after assuming the material parameters obtained by the second calibration point. Two different loading conditions are performance: pure shear and shear/tensile. The performance of some parameters as equivalent plastic strain and displacement at fracture as well as the ability to predict the correct site to crack initiation are evaluated for each calibration point.

5.1 Evolution of the equivalent plastic strain and damage parameter

The equivalent plastic strain and the displacement at fracture are very important parameters to evaluate the performance and accuracy of the constitutive models as well as the evolution of the damage parameter during all the process. Figure 8 and Figure 9 show the evolution of both damage parameter and equivalent stress at the critical point of the butterfly specimen, taken hand both material parameters determined by the first and second calibration point. Regarding the numerical results for the first calibration point, the GTN model with Xue shear mechanism has presented very conservative, predicting the beginning of the failure for a displacement equal to $u_f = 0.37\ mm$, which is in disagreement with the experimental data. Besides that, the GTN model with N&H shear mechanism and $k = 1.1$ has presented the best performance, predicting the failure for a displacement near of the experimental data, $u_f = 0.86\ mm$. Regarding the value of the equivalent plastic strain at fracture, the N&H shear mechanism also presented the best results. Furthermore, in combined shear/tensile loading condition, the best performance can be highlight for the GTN model with Xue shear mechanism, regarding the equivalent plastic strain and displacement at fracture (see Table 3).

Taken hand of the numerical results for the second calibration point (see Figure 9 and Table 4), during the calibration procedure, each shear mechanism presented a different value for the critical damage variable. Hence, in pure shear loading condition, the results for the Xue shear mechanism performance well, regarding the level of the equivalent plastic strain at fracture. This parameter calculated by N&H shear mechanism was very high and in disagreement with the expected value. In combined loading condition, the value of the equivalent plastic strain by N&H shear mechanism also presented very high but the mechanism predicted the failure for a displacement close to the experimental value. The Xue shear mechanism, in this case, presented both equivalent plastic strain and displacement at fracture, in disagreement with the experimental data.

Regarding the numerical results for both shear mechanism using the material parameters calibrated in different loading condition, we can conclude that in pure shear loading condition, the results presented by Xue, taken hand the second

calibration point, performance well in terms of the level of the equivalent plastic strain and displacement at fracture. In Combined loading condition, the analysis is not so simple and the results presented by Xue using the first calibration point are quite satisfying. In the other hand, the results by N&H shear mechanism, using the second calibration point can also be accurate, in terms of the displacement at fracture. Hence, the assessment of the prediction of the correct fracture location can be used as a complementary validation.

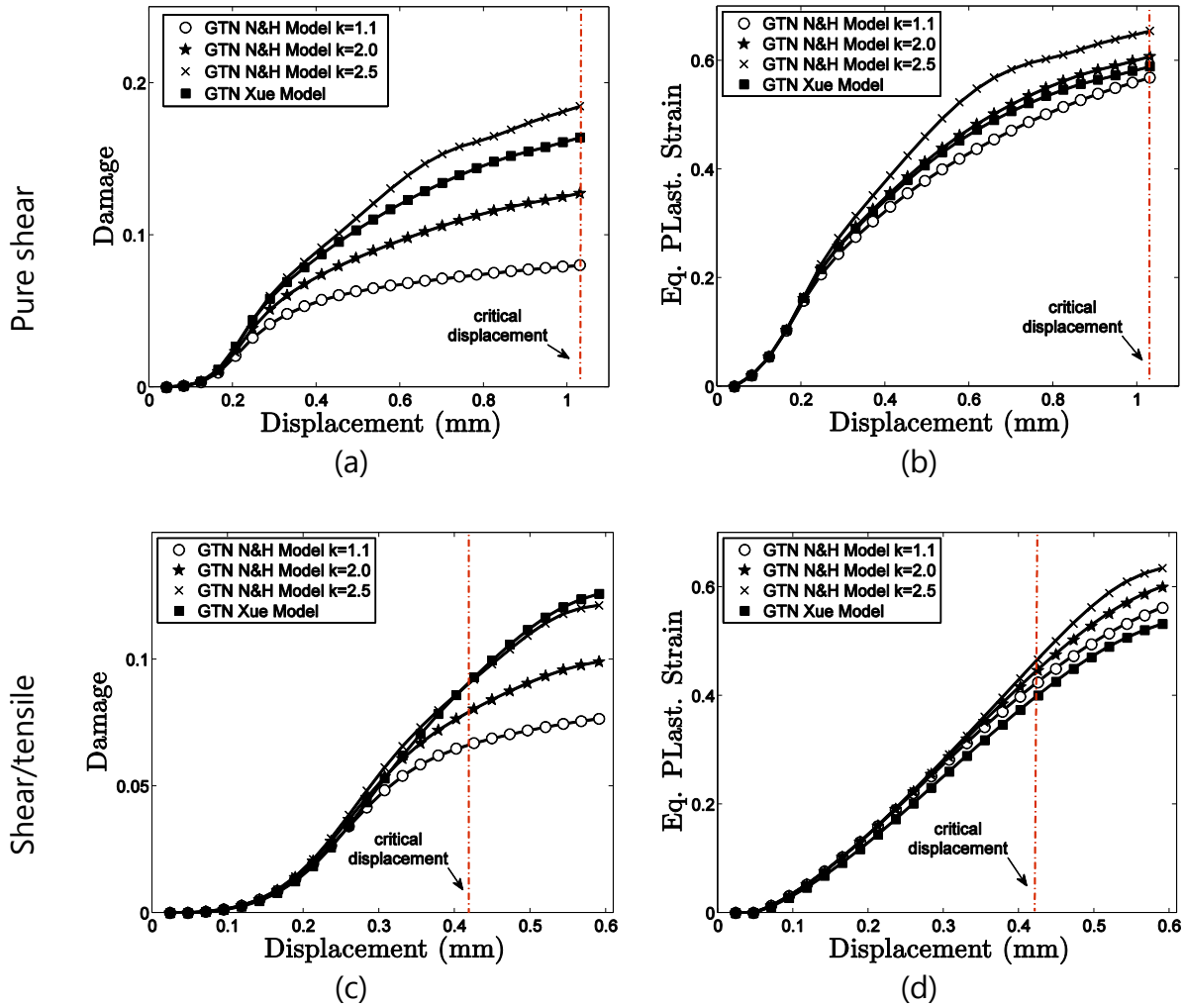

Figure 8. Evolution of the damage parameter and equivalent plastic strain. Based on the first calibration point.

Angle	Experimental data			Numerical results					
	u_f	$\bar{\varepsilon}^p$		k	u_f	$\bar{\varepsilon}^p$	η_{av}	θ_{av}	f
0°	***1.03***	***0.36***	*N&H*	***1.1***	***0.86***	***0.53***	***0.022***	***0.061***	***0.076***
			N&H	2.0	0.45	0.38	0.022	0.060	0.076
			N&H	2.5	0.37	0.35	0.022	0.060	0.076
			Xue	---	***0.37***	***0.32***	***0.021***	***0.057***	***0.076***
10°	***0.42***	***0.50***	*N&H*	***1.1***	***0.59***	***0.56***	***0.241***	***0.477***	***0.076***
			N&H	2.0	0.40	0.41	0.245	0.485	0.076
			N&H	2.5	0.37	0.38	0.246	0.488	0.076
			Xue	---	***0.37***	***0.34***	***0.257***	***0.507***	***0.076***

Table 3: Numerical results for butterfly specimen. Based on the first calibration point.

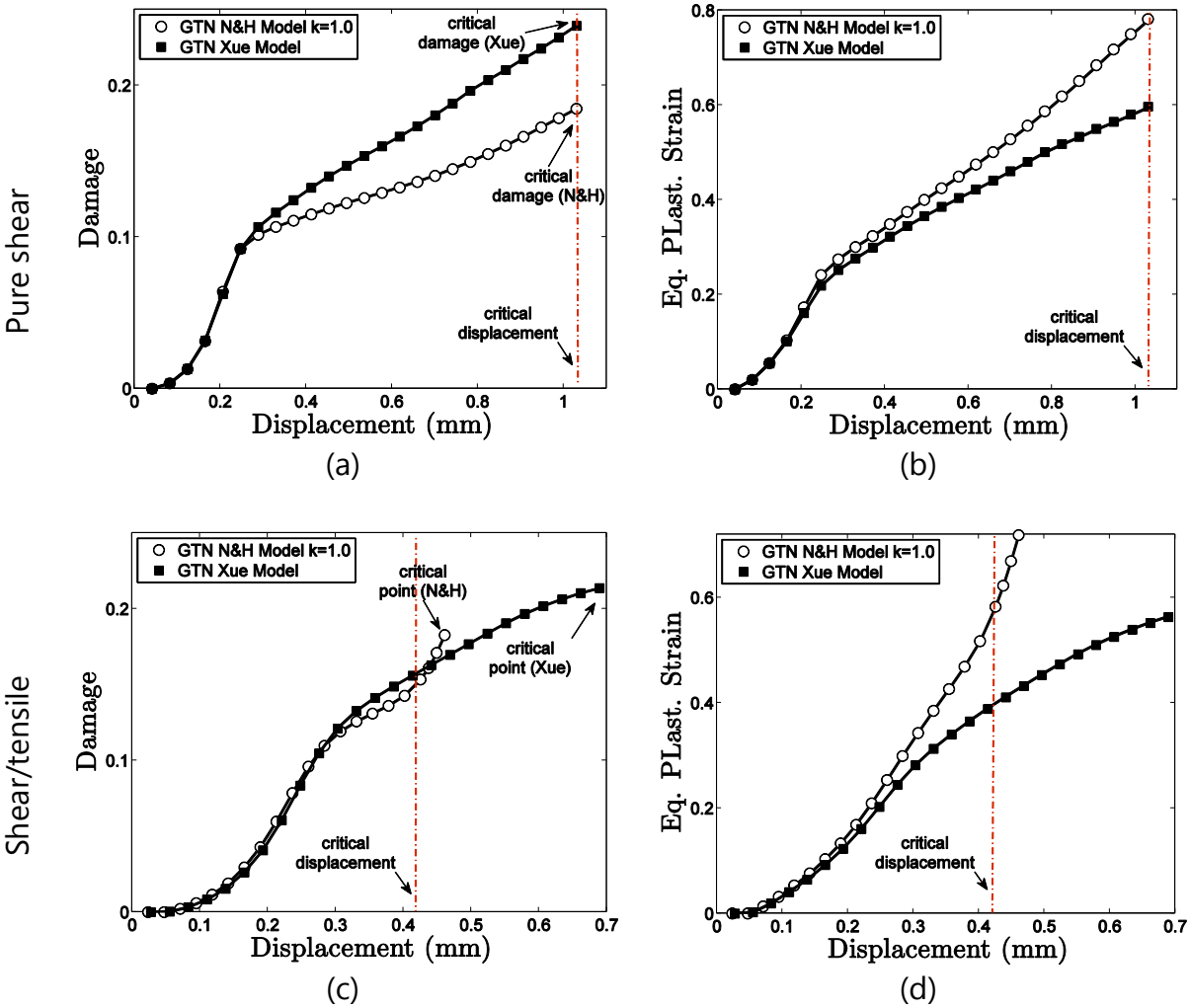

Figure 9. Evolution of the damage parameter and equivalent plastic strain. Based on the second calibration point.

Angle	Experimental data			Numerical results					
	u_f	$\bar{\varepsilon}^p$		k	u_f	$\bar{\varepsilon}^p$	η_{av}	θ_{av}	f
0°	***1.03***	***0.50***	*N&H*	***1.0***	***1.03***	***0.78***	***0.022***	***0.061***	***0.24***
			Xue	***---***	***1.03***	***0.59***	***0.021***	***0.057***	***0.19***
10°	***0.42***	***0.36***	*N&H*	***1.0***	***0.46***	***0.71***	***0.241***	***0.477***	***0.24***
			Xue	***---***	***0.69***	***0.56***	***0.257***	***0.507***	***0.19***

Table 4: Numerical results for butterfly. Based on the second calibration point.

5.2 Prediction of the correct fracture location

Another important data to be analyzed in order to validate the accuracy of both shear mechanism in two different calibration point is the ability to predict the correct fracture location. Researches as Reis et al. (2010) and Malcher et al. (2010) have shown that the shear mechanisms already proposed in literature, fail in the prediction of the correct location to crack formation when combined loading condition is applied. Based on experimental tests performed by Bai (2008), using the butterfly specimen, it can be observed that in pure shear loading condition, the micro crack is initially formatted in the surface of the critical zone. However, when combined shear/tensile loading condition is applied, the crack is formatted in the middle of the thickness and growth toward the surface of the critical zone. Figure 10 and Figure 11 present the contour of the damage parameter at fracture for both calibration point. We can conclude that, in pure shear loading condition, both shear mechanisms have ability to predict the correct site to crack formation independent of the calibration point. However, in combined loading condition, only the contours obtained by the material parameters calibrated in the second calibration point, agree with the experimental evidence. Hence, regarding both analyze, evolution of the internal variable at fracture and ability to predict the correct fracture location, we can suggest that the second calibration point presented the best results.

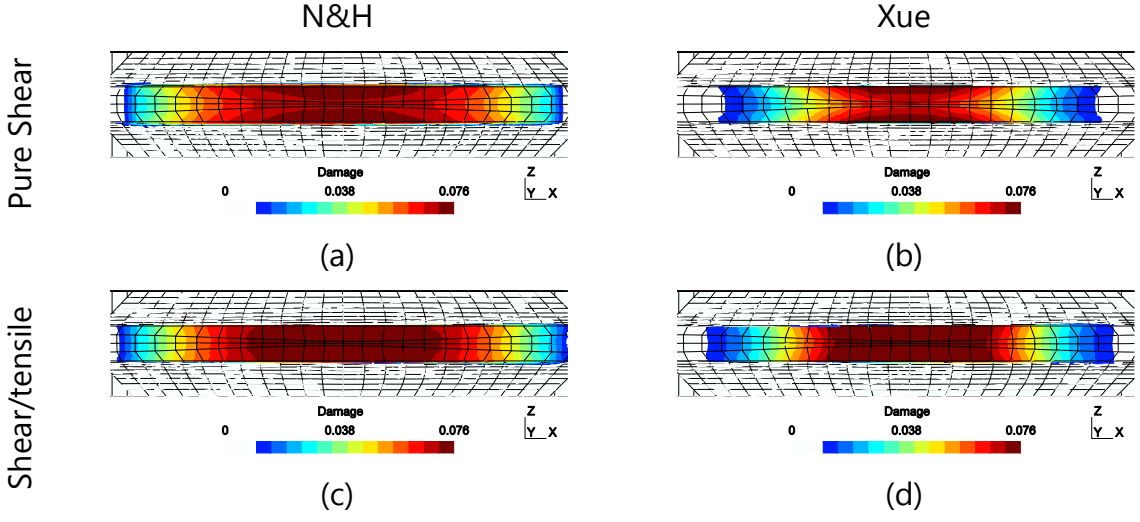

Figure 10. Contour of the damage parameter for both shear mechanisms. Based on the first calibration point.

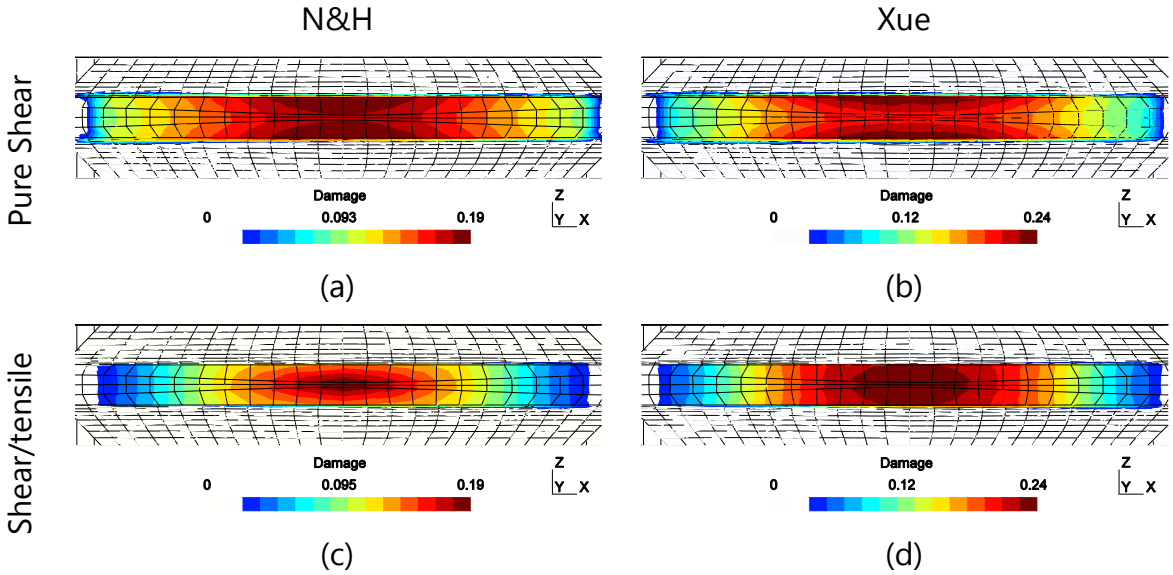

Figure 11. Contour of the damage parameter for both shear mechanisms. Based on the second calibration point.

6 CONCLUSIONS

In this paper, an assessment of two different shear mechanisms was performance taken hand the set of material parameters, calibrated in two different points. A point in high stress triaxiality as well as another point in pure shear loading condition was chosen to performance the calibration procedure. Besides that, numerical results were done regarding two loading condition, as: pure shear and combined shear/tensile. The evolution of the equivalent plastic strain, the damage parameter and displacement at fracture were analyzed as well as the ability to predict the correct site to crack initiation. The results obtained, highlight that for coupled damage models, the point chosen to be used as calibration point exerts a great influence on numerical results. The accuracy of the coupled damage models is strongly dependent of the calibration point and for these models, the loading condition to be validated has to be close to the loading condition selected to be used as calibration point. For this analyze, regarding all numerical results, the second calibration point has the best results and can be suggested to be used when predominant shear loading condition is present.

7 ACKNOWLEDGEMENTS

Lucival Malcher is supported by Portuguese Science and Technology Foundation (FCT), under scholarship number SFRH/BD/45456/2008. Fábio Reis is supported by Portuguese Science and Technology Foundation (FCT), under scholarship number SFRH/BD/60887/2009. The authors acknowledge the support of Portuguese Science and Technology Foundation (FCT) under grant with reference PTDC/EME-TME/71325/2006.

REFERENCES

Andrade Pires, F.M., César de Sá, J.M.A., Costa Sousa, L., Natal Jorge, R.M., Numerical Modeling of ductile plastic damage in bulk metal forming, *International Journal of Mechanical Sciences*, 45:273–294, 2003.

Bai, Y., Effect of Loading History on Necking and Fracture. Ph.D Thesis, *Massachusetts Institute of Technology*, 2008.

Besson, J., Steglich, D. and Brocks, W., Modeling of crack growth in round bars and plane strain specimens. *International Journal of Solids and Structures*, 38(46–47):8259–8284, 2001.

Besson, J., Continuum Models of Ductile Fracture: A Review. *International Journal of Damage Mechanics*, 19:3-52, 2010.

Butcher, C., Chen, Z., Bardelcik, A., Worswick M., Damage-based finite-element modeling of tube hydroforming. *International Journal of Fracture*, 155:55–65, 2009.

Chaboche, J.L., Anisotropic Creep Damage in the Framework of Continuum Damage Mechanics. *Nuclear Engineering and Design,*79: 309–319, 1984.

Chaboche, J.L., Damage mechanics. *In: Milne, I., Ritchie, R.O. and B. Karihaloo (eds.) Comprehensive Structural Integrity*, vol. 2. Elsevier-Pergamon, pp. 213–284, 2003.

Chaboche, J.L., Boudifa, M., Saanouni, K., A CDM approach of ductile damage with plastic compressibility. *International Journal of Fracture*, 137:51–75, 2006.

De Souza Neto, E.A., Peri´c, Owen, D.R.J., Computational methods for plasticity: theory and applications. *John Wiley & Sons Ltd*, 2008.

Engelen, Roy A.B., Plasticity-induced Damage in Metals / nonlocal modelling at finite strains. PhD Thesis – Eindhoven : Technische Universiteit Eindhoven, 2005.

Gurson, A.L., Continuum Theory of ductile rupture by void nucleation and growth - Part I. Yield criteria and flow rules for porous ductile media. *J. Engrg. Mat. Tech.,* 99:2-15, 1977.

Krajčinović, D., Fonseka, G.U., The Continuous Damage Theory of Brittle Materials – Part 1: General Theory. *J. Appl. Mech.*, 48, 809–815, 1981.

Lemaitre, J., A continuous damage mechanics model for ductile fracture. *Journal of Engineering Materials and Technology - Trans. of the ASME*, 107:83–89, 1985.

Lemaitre, J., Chaboche, J.L., Mechanics of Solid Materials. Cambridge Univ. Press, 1990.

Malcher, L. ; Andrade Pires, F.M. ; César de Sá, J.M.A., An Assessment of Isotropic Damage Constitutive Models under High and Low Stress Triaxialities. *International Journal of Damage Mechanics*, *Submitted for publication*, 2010.

McClintock, F. A., A Criterion for Ductile Fracture by the Growth of Holes. J. Appl. Mech., 35, 363–371, 1968.

Murakami, S., & Ohno, N., A Continuum Theory of Creep and Creep Damage. Pages 422–443 of: Ponter, A.R.S. (ed), Proceedings of the IUTAM Symposium on Creep in Structures, Leicester, Berlin, 1981.

Nahshon, K., Hutchinson, J., Modification of the Gurson model for shear failure. *European Journal of Mechanics A/Solids,* 27:1–17, 2008.

Pineau, A., Review of fracture mechanisms and local approaches to predicting crack resistance in low strength steels. In: François, D. et al. (ed.) Advances in Fracture Researches. New-York, Pergamon Press, ICF5. Cannes, 1981.

Reis, F.J.P.; Malcher, L. ; Andrade Pires, F.M. ; César de Sá, J.M.A., A modified GTN model for the prediction of ductile fracture at low stress triaxialities. *International Journal of Structural Integrity, Accepted*, 2010.

Rice, J. R., Tracey, D., M., On the ductile enlargement of voids in triaxial stress fields. *Journal of the Mechanics and Physics of Solids*, 17:201–217, 1969.

Rousselier's, G., Finite deformation constitutive relations including ductile fracture damage. In: Nemat-Nasser (ed.) Three-Dimensional Constitutive Relations and Ductile Fracture. North-Holland Publ. Comp., 1981 pp. 331–355, 1980.

Rousselier's, G., Ductile fracture models and their potential in local approach of fracture. *Nuclear Engineering and Design* 105: 97–111, 1987.

Simo, J.C., & Hughes, T.J.R., Computational Inelasticity. New York: Springer-Verlag.

Teng, X. (2008). Numerical prediction of slant fracture with continuum damage mechanics. *Engineering Fracture Mechanics*, 75:2020–2041, 1998.

Tvergaard, V. and Needleman, A., Analysis of the cup-cone fracture in a round tensile bar. *Acta Met.* 32:157–169, 1984.

Xue, L., Ductile Fracture Modeling – Theory, Experimental Investigation and Numerical Verification, Ph.D Thesis, *Massachusetts Inst. of Technology*, 2007.